단일방향 및 크로스-플라이 섬유강화 복합체에서의 동적균열 전파모사

Simulation of Dynamic Crack Propagation in Uni-Directional and Cross-Ply Fiber-Reinforced Composites

황 찬 규†
Hwang, Changyu
(논문접수일 : 2008년 4월 7일 ; 심사종료일 : 2008년 5월 6일)

요 지

이 논문에서는 단일방향 및 크로스-플라이 섬유강화 복합재에서의 동적 균열 전파를 모사하기 위해 특별히 고안된 스펙트랄 방법의 정식화와 수치적 구현 방법에 대해 제시한다. 이 방법은 균열면에서 작용하는 힘과 변위 사이의 스펙트랄 관계식에 기초하고 있고, 재료는 횡등방성 고체로 가정된다. 본 논문에서 제안된 방법에 의해 섬유보강 복합재에서 전파하는 균열문제가 대해 검토 해석되며, 실험 및 문헌에 나와 있는 결과와 비교된다. 이 방법은 FRP 보강 철근 콘크리트 구조물에서의 균열해석문제에 직접 적용이 가능하다.

핵심용어 : 스펙트랄 방법, 횡등방성 고체, 섬유보강복합재, 동적균열전파

Abstract

This paper presents the formulation and numerical implementation of a spectral scheme specially developed to simulate dynamic fracture events in unidirectional and cross-ply fiber-reinforced composites. The formulation is based on the spectral representation of the transversely isotropic elastodynamic relations between the traction stresses along the fracture plane and the resulting displacements. Example problem of dynamically propagating cracks in fiber-reinforced composites is investigated and compared with reference solutions available in the literature and/or experimental observations. This scheme can be directly applicable to the interfacial fracture analysis in the FRP reinforced concrete structures.

Keywords : *Spectral method, transversely isotropic solid, fiber-reinforced composites, dynamic crack propagation*

1. Introduction

The most notorious example of dynamic failure of composite structures is undoubtedly the extensively studied impact-induced delamination(Abrate, 1998), in which substantial subsurface damage can take place in a composite laminate without apparent subsurface damage in the vicinity of the impact point. Rapid propagation of planar cracks has also been observed in thicker uni- and multidirectional composites(Lambros and Rosakis, 1997), including the appearance of intersonic crack speeds under shear-dominated loading conditions(Coker and Rosakis, 1998). These various observations have motivated the present development of an efficient numerical scheme able to investigate in great details a wide range of fundamental dynamic fracture problems involving a planar crack embedded in an infinite linearly elastic unidirectional or cross-ply composite medium and subjected to any quasi-static or dynamic loading conditions. The spectral form of the

† 책임저자, 정회원 · 서울벤처정보대학원대학교 유비쿼터스시스템학과 교수
Tel: 02-3470-5281 ; Fax: 02-523-6767
E-mail: changyu.hwang@gmail.com

• 이 논문에 대한 토론을 2008년 10월 31일까지 본 학회에 보내주시면 2008년 12월호에 그 결과를 게재하겠습니다.

boundary integral formulation presented in this paper is directly inspired from previous developments of the numerical scheme used in the analysis of 2D and 3D fundamental dynamic fracture problems in homogeneous (Geubelle and Rice, 1995) and bimaterial(Geubelle and Breitenfeld, 1997; Breitenfeld and Geubelle, 1998) media. The spectral formulation relies on the elastodynamic relations, expressed in the Fourier domain, between the traction stresses acting along the fracture plane and the associated displacement and velocity components. In Section 2, we start with a brief review of the elastodynamic relations for a transversely isotropic material, then summarize the derivation of the corresponding 2D spectral formulation and implementation. Section 3 is dedicated to the simulation of subsonic and intersonic crack propagation in unidirectional and cross-ply composite media and to a comparison with the experimental observations obtained by Coker and Rosakis(1998).

2. Transversely isotropic spectral formulation

The spectral formulation developed hereafter aims at the accurate and efficient solution of two types of 2D dynamic fracture problems in fiber-reinforced composite media. The first type is concerned with the dynamic failure of unidirectional composites, for which the symmetry axis(i.e., the fiber direction) is either perpendicular(Fig. 1a) to the crack front. The second type of fracture problem considered in this paper is associated with the dynamic delamination of a[0/90] cross-ply composite(Fig. 1b), with the planar crack propagating along the planar interface. In addition to the two-dimensionality of the displacement, $u_i(x_1,x_2,t)$ and stress $\sigma_{ij}(x_1,x_2,t)$ fields, we further assume that the dynamic response and failure of the composite is adequately captured by the homogenized anisotropic elasticity theory, thereby neglecting the heterogeneity associated with the multi-phase microstructure.

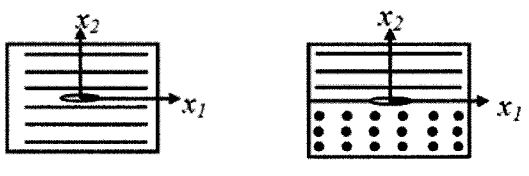

(a) (b)

Figure 1 Fiber-reinforced composites: (a) fibers in x_1-direction, (b) bimaterial system.

We start the derivation of the spectral formulation from the displacement form of the elastodynamic relations, which, for the two special fiber orientations considered here, take a simpler form allowing for the decoupling of the in-plane and out-of-plane motions. For the 0° case, the in-plane motion is described by

$$c_{11}\frac{\partial^2 u_1}{\partial x_1^2}+c_{66}\frac{\partial^2 u_1}{\partial x_2^2}+(c_{12}+c_{66})\frac{\partial^2 u_2}{\partial x_1 \partial x_2}=\rho\frac{\partial^2 u_1}{\partial t^2} \tag{1}$$

$$c_{66}\frac{\partial^2 u_2}{\partial x_1^2}+c_{22}\frac{\partial^2 u_2}{\partial x_2^2}+(c_{12}+c_{66})\frac{\partial^2 u_1}{\partial x_1 \partial x_2}=\rho\frac{\partial^2 u_2}{\partial t^2} \tag{2}$$

and the out-of-plane motion by

$$c_{66}\frac{\partial^2 u_3}{\partial x_1^2}+\frac{1}{2}(c_{22}-c_{23})\frac{\partial^2 u_3}{\partial x_2^2}=\rho\frac{\partial^2 u_3}{\partial t^2} \tag{3}$$

The five elastic constants c_{11}, c_{22}, c_{12}, c_{23} and c_{66} entering Eqs. (1~3) define the constitutive relations for an isotropic medium with its symmetry axis aligned with the x_1 axis:

$$\begin{Bmatrix}\sigma_{11}\\ \sigma_{22}\\ \sigma_{33}\\ \sigma_{23}\\ \sigma_{13}\\ \sigma_{12}\end{Bmatrix}=\begin{bmatrix}c_{11} & c_{12} & c_{12} & 0 & 0 & 0\\ c_{12} & c_{22} & c_{23} & 0 & 0 & 0\\ c_{12} & c_{23} & c_{22} & 0 & 0 & 0\\ 0 & 0 & 0 & \frac{c_{22}-c_{23}}{2} & 0 & 0\\ 0 & 0 & 0 & 0 & c_{66} & 0\\ 0 & 0 & 0 & 0 & 0 & c_{66}\end{bmatrix}\begin{Bmatrix}\varepsilon_{11}\\ \varepsilon_{22}\\ \varepsilon_{33}\\ 2\varepsilon_{23}\\ 2\varepsilon_{13}\\ 2\varepsilon_{12}\end{Bmatrix} \tag{4}$$

For an isotropic solid, these elastic constants can be expressed in terms of the Lamé constants λ and μ as

$$c_{11}=c_{22}=\lambda+2\mu,\quad c_{12}=c_{23}=\lambda,\quad c_{66}=\mu \tag{5}$$

Transversely isotropic materials are characterized by three fundamental bulk wave speeds: the shear wave speed, c_s, the dilatational wave speed in the fiber direction, $c_d^{(1)}$, and the dilatational wave speed normal to fibers, $c_d^{(2)}$, respectively defined as

$$c_s = \sqrt{\frac{c_{66}}{\rho}}\ ,\quad c_d^{(1)} = \sqrt{\frac{c_{11}}{\rho}}\ ,\quad c_d^{(2)} = \sqrt{\frac{c_{22}}{\rho}} \tag{6}$$

where ρ denotes the density of the material.

The basic steps leading to the derivation of the spectral formulation for a transversely isotropic material are somewhat similar to those used by Breitenfeld and Geubelle(1998) in the bimaterial isotropic case. Only the important relations corresponding to the 0° case are indicated here. The particular form of the spectral formulation used here is the so-called *independent formulation* introduced by Geubelle and Breitenfeld(1997), which has been shown to have better accuracy and stability than the original *combined formulation* presented by Geubelle and Rice(1995) under shear or mixed-mode loading conditions.

Let $\tau_i(x_1,t) = \sigma_{i2}(x_1, x_2 = 0, t)$ denote the dynamic traction stresses acting on the fracture plane $x_2 = 0$, and $u_i^{\pm}(x_1,t) = u_i\left(x_1, x_2 = 0^{\pm}, t\right)$ the boundary displacements. The fundamental form of the elastodynamic equations used in this work is

$$\tau_i(x_1,t) = \tau_i^o(x_1,t) \mp V_{ik}^{\pm}\frac{\partial u_k^{\pm}(x_1,t)}{\partial t} + f_i^{\pm}(x_1,t) \tag{7}$$

where $\tau_i^o(x_1,t)$ denotes the externally applied traction stress that would exist on the fracture plane if no crack was present; the second term, often referred to as the radiation term, corresponds to the instantaneous response of the material; the last term incorporates the dynamic effects associated with the non-uniform motion of the fracture surfaces. The superscripts "+" and "-" indicate quantities associated with the upper and lower materials, respectively, and are omitted unless required for clarity. In Eq. (7), V_{ij} denote the components of a diagonal matrix containing material properties

$$V_{11} = \frac{c_{66}}{c_s}\ ,\quad V_{22} = \frac{c_d^{(2)}}{c_s^2}c_{66}\ ,\quad V_{33} = \frac{c_{66}}{\beta\, c_s} \tag{8}$$

where $\beta = \sqrt{2c_{66}/(c_{22}-c_{23})}$ ($\beta = 1$ for isotropic media). The last term in Eq. (7), $f_i(x_1,t)$, is the convolution term and is expressed in the spectral domain as a time convolution between its Fourier coefficients $F_i(t;q)$ and the Fourier coefficients $U_i^{\pm}(t;q)$ of the boundary displacements $u_i^{\pm}(x_1,t)$ as

$$\begin{aligned}
F_1^{\pm}(t;q) &= \pm c_{66}^{\pm}|q|\int_0^t H_{11}\left(|q|c_s^{\pm}t'\right)U_1^{\pm}(t-t';q)|q|c_s^{\pm}dt' \\
&+ ic_{66}^{\pm}|q|\left(2-\frac{2+\eta^{(2)\pm}+\eta^{(3)\pm 2}}{1+\eta^{(2)\pm}}\right)U_2^{\pm}(t;q) \\
&+ ic_{66}^{\pm}|q|\int_0^t H_{12}\left(|q|c_s^{\pm}t'\right)U_2^{\pm}(t-t';q)\ |q|c_s^{\pm}dt'
\end{aligned} \tag{9}$$

$$\begin{aligned}
F_2^{\pm}(t;q) &= \mp c_{66}^{\pm}|q|\int_0^t H_{22}\left(|q|c_s^{\pm}t'\right)U_2^{\pm}(t-t';q)|q|c_s^{\pm}dt' \\
&- ic_{66}^{\pm}|q|\left(2-\frac{2+\eta^{(2)\pm}+\eta^{(3)\pm 2}}{1+\eta^{(2)\pm}}\right)U_1^{\pm}(t;q) \\
&- ic_{66}^{\pm}|q|\int_0^t H_{12}\left(|q|c_s^{\pm}t'\right)U_1^{\pm}(t-t';q)\ |q|c_s^{\pm}dt'
\end{aligned} \tag{10}$$

$$F_3^{\pm}(t;q) = \mp\frac{c_{66}^{\pm}}{\beta^{\pm}}|q|\int_0^t H_{33}\left(|q|c_s^{\pm}t'\right)U_3^{\pm}(t-t';q)|q|c_s^{\pm}dt' \tag{11}$$

where q is the spectral mode number; t is time; i is the imaginary number; $\eta^{(1)} = \sqrt{c_{11}/c_{66}}$;

$\eta^{(2)} = \sqrt{c_{22}/c_{66}}$; $\eta^{(3)} = \sqrt{c_{12}/c_{66}}$.

One of the major advantages of the spectral method is associated with the non-singular character of the convolution kernels H_{ij} entering Eqs. (9~11). In the 0° case(see Fig. 1a), H_{ij} are defined as

$$H_{11}(T) = L^{-1}\left[\frac{\sqrt{s^2+\eta^{(1)2}}\sqrt{\left(\eta^{(2)}\sqrt{s^2+\eta^{(1)2}}+\sqrt{1+s^2}\right)^2-\left(1+\eta^{(3)2}\right)^2}}{\eta^{(2)}\sqrt{s^2+\eta^{(1)2}}+\sqrt{1+s^2}}-s\right] \tag{12}$$

$$H_{12}(T)=$$

$$L^{-1}\left[\frac{\eta^{(2)}\sqrt{s^2+\eta^{(1)2}}+\sqrt{1+s^2}\left(2+\eta^{(3)2}\right)}{\eta^{(2)}\sqrt{s^2+\eta^{(1)2}}+\sqrt{1+s^2}}+\frac{2+\eta^{(2)}+\eta^{(3)2}}{1+\eta^{(2)}}\right] \tag{13}$$

$$H_{22}(T)=$$

$$L^{-1}\left[\frac{\eta^{(2)}\sqrt{1+s^2}\sqrt{\left(\eta^{(2)}\sqrt{s^2+\eta^{(1)2}}+\sqrt{1+s^2}\right)^2-\left(1+\eta^{(3)2}\right)^2}}{\eta^{(2)}\sqrt{s^2+\eta^{(1)2}}+\sqrt{1+s^2}}-\eta^{(2)}s\right] \tag{14}$$

where $s=p/c_s|q|$ and $\hat{f}(p)$ denotes the Laplace transform of $f(t)$. The convolution kernels are readily inverted back to the time domain using conventional numerical Laplace inversion algorithms. The convolution kernel for the out-of-plane motion, H_{33}, is identical to that entering the isotropic problem, and is given by $H_{33}(T)=J_1(T)/T$, where $J_1(T)$ denotes the Bessel function of the first kind. The convolution kernels are illustrated in Fig. 2 for a Graphite/Epoxy composite material with c_{11}=82GPa, c_{22}=11.1GPa, c_{12}=4.0GPa, c_{23}=4.9 GPa and c_{66}=3.6GPa. As apparent in Fig. 2, the convolution kernels are non-singular, oscillating and decaying functions, and do not therefore require the special treatment associated with the(hyper)singular kernels encountered in more conventional boundary integral formulations.

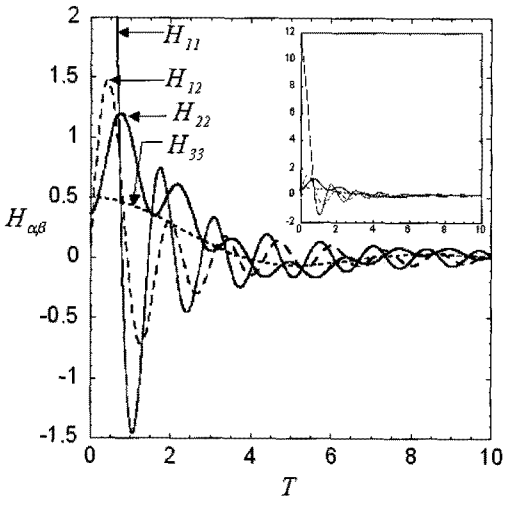

Figure 2 Convolution kernels entering the spectral formulation for a graphite/epoxy material.

To complete the spectral formulation Eqs. (7~11), three components(appropriate interface conditions, a time stepping scheme and cohesive-based failure model) are needed. Firstly, appropriate interface conditions must be incorporated to link the elasto-dynamic solutions of the two half spaces described by Eq. (7). Four interface conditions must be considered: 1) the non-failing region, in which the traction stresses and displacements are continuous across the interface; 2) the cohesive failure zone, where the traction stresses are equal to the(possibly decaying) strength of the material; 3) the traction-free crack region, in which the traction stresses are set to zero; and 4) the possibility of spontaneous contact between the crack faces, where the interface conditions correspond to the continuity of the normal tractions and the absence of material interpenetration. See Section 3 in Breitenfeld and Geubelle(1998) for the implementation of the interface conditions. Secondly, a time stepping scheme must be introduced to integrate over time the velocity distribution derived from Eq. Eq. (7) and obtain the displacement solution entering the convolution relations Eqs. (9~11). Finally, in order to simulate dynamic fracture problems involving the spontaneous initiation, propagation and arrest of a crack, a cohesive-based failure model must be introduced to relate the strength of the material along the fracture plane to the displacement and/or velocity discontinuities. Among the wide range of cohesive models that can be incorporated in the spectral scheme, we use hereafter a relatively simple rate-independent coupled cohesive failure model, which relates the normal and shear strengths along the fracture plane to the normal(δ_n) and tangential(δ_s) displacement discontinuities across the fracture plane as

$$\tau_{n,s}^{str}=\tau_{n,s}^{c}\left\langle 1-\sqrt{\left(\frac{\delta_n}{\delta_n^c}\right)^2+\left(\frac{\delta_s}{\delta_s^c}\right)^2}\right\rangle \tag{15}$$

where $\langle a \rangle = a$ if $a > 0$ and $= 0$ otherwise; τ_n^c and τ_s^c denote the intact tensile and shear strengths of the fracture plane, while δ_n^c and δ_s^c correspond to the critical values of the normal and shear crack opening displacements beyond which complete failure is achieved. Note that τ_n^{str} and τ_s^{str} are the normal and shear strength of the interface. The numerical implementation of the spectral scheme for the transversely isotropic problem is similar to that used in the isotropic case by Breitenfeld and Geubelle (1998). For completeness purpose, let us indicate that it involves the discretization of a period X of the fracture plane by N uniformly spaced grid points separated by X/N. A Fourier series representation of the displacements and dynamic stress distribution is introduced as

$$\left[u_j^{\pm}(x_1,t),\, f_j^{\pm}(x_1,t)\right] = \sum_{k=-N/2}^{k=N/2}\left[U_j^{\pm}(t),\, F_j^{\pm}(t)\right] exp[2\pi ikx/X] \tag{16}$$

with the conversion between spectral and real domains performed efficiently through an FFT algorithm, using the N grid points as sampling points. The aforementioned time stepping scheme is explicit. The time step size is therefore dictated by the classical Courant stability condition.

3. Subsonic and intersonic crack propagation

As indicated in the introductory section, observations of dynamic failure in unidirectional graphite/epoxy composites performed recently by Coker and Rosakis(1998) have yielded somewhat unexpected results. Under dynamic tensile(mode I) loading, subsonic crack motion(i.e., at speeds below the Rayleigh wave speed) is observed, and, unlike in the homogeneous case for which tensile cracks hardly exceed 0.4 to 0.5 c_R due to branching instabilities, mode I cracks in unidirectional composites can achieve propagation speeds approaching c_R. When the composite is subjected to dynamic shear(mode II) loading, cracks tend to enter the intersonic regime, for which the crack velocity v_c exceeds the shear wave speed c_S of the surrounding material, but remains below the dilatational wave speed $c_d^{(I)}$. This fracture response of unidirectional composites is reminiscent of recently observed intersonic crack motion in homogeneous isotropic specimens subjected to shear loading(Rosakis, Samudrala and Coker, 1999). However, unlike in the isotropic case where a weak plane has to be introduced ahead of the pre-crack to prevent the shear-loaded crack from kinking out of its original plane, weak planes exist naturally in unidirectional composites parallel to the fiber direction. Any deviation from planar crack motion is faced with a substantial energetic penalty associated with the fiber breakage and pullout processes. To investigate the intersonic motion of a crack in a unidirectional composite, Huang, Wang, Liu and Rosakis(1999) have presented an asymptotic analysis of the near-tip fields for a steadily propagating mode-II crack, showing the existence in the intersonic range of a critical crack tip velocity characterized by a non-vanishing energy release rate. The steady-state intersonic mode-II crack problem was also studied by Broberg(1999), who also determined the energy flow into the process region using the Barenbhalt cohesive failure model. In a recent numerical analysis, Geubelle and Kubair (2000) have used the isotropic version of the spectral scheme to study various issues associated with the subsonic to intersonic transition in isotropic systems under pure mode II and mixed-mode conditions. Building on the success of this analysis, we show in this section how the spectral scheme developed above can be used to study accurately the subsonic and intersonic fracture of unidirectional graphite/epoxy composites and reproduce the experimental results of Coker and Rosakis. While we limit our investigation to the pure mode I and mode II loading cases, we study two material systems: the homogeneous 0° case, and the bimaterial [0/90] problem(Fig. 1). The model

dynamic fracture problem simulated hereafter is schematically shown in Fig. 3. It consists of a pre-stressed graphite/epoxy specimen subjected to uniform tensile(θ=0°) or shear(θ=90°) loading σ_o =18Mpa. At time t=0, a crack of initial length $a_o = L/8$(where L=0.2m denotes the discretized portion of the fracture plane) is introduced on the left side of the domain. Due to the dynamic stress concentration building up in its vicinity, the right crack tip starts to propagate along the x_1-axis, while the left crack tip is kept stationary. For simplicity we assume that the tensile and shear failure properties of the composite along the fracture plane are equal, both with regards to the strength values($\tau_n^c = \tau_s^c = \tau^c$ =36Mpa) and the critical values of the crack opening displacements ($\delta_n^c = \delta_s^c = \delta^c$ =26.3μm) entering the cohesive failure model described in Eq. (15). 2048 equally spaced grid points are used to discretize the fracture plane, and the time step is chosen as $c_s \Delta t = 0.1 \Delta x$, where Δx denotes the grid point spacing. In all the simulations of spontaneous crack propagation, special care was taken to capture with cohesive failure zone with sufficient accurately(typically, with at least 10 sampling points). The elastic wave speeds for the graphite/epoxy composite are listed in Table 1 for the two fiber orientations considered here. Fig. 4 illustrates the evolution of the crack tip speed as a function of crack tip position for the unidirectional composite specimens subjected to both mode-I and mode-II loading. The results relative to the 0° unidirectional composite are directly relevant to the experiments

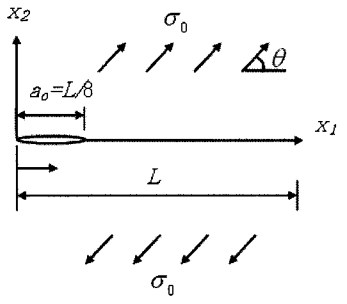

Figure 3 Schematic of the dynamic crack propagation problem

Table 1 The elastic wave speeds 0° and 90° graphite/epoxy composite

Wave speeds	Fibers parallel to x_1-axis	Wave speeds	Fibers parallel to x_3-axis
$c_d^{(1)}$	7450m/s	$c_d^{(1)}$	2740m/s
$c_d^{(2)}$	2740m/s	$c_d^{(2)}$	2740m/s
c_s	1560m/s	c_s	1448m/s
c_R	1548m/s	c_R	1433m/s

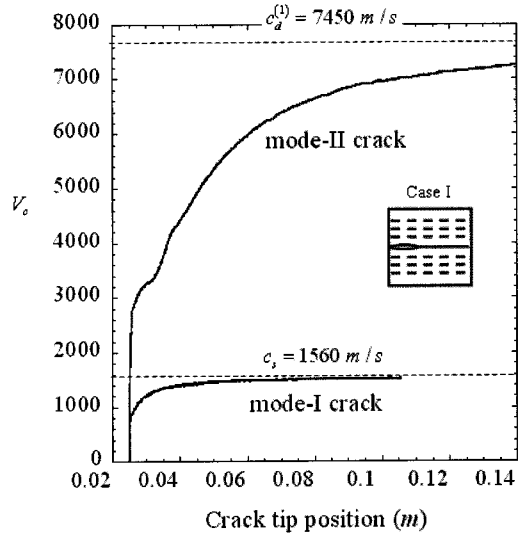

Figure 4 Crack tip speed(V_c) as a function of crack tip position for mode-I and mode-II cracks in case I: unidirectional 0° case.

performed by Coker and Rosakis(1998), although the impact loading used in their experiments is quite different from the uniform pre-loading used in our model dynamic fracture problem.

As was the case in their experiments(see Fig. 19 of Coker and Rosakis(1998)), the mode I loaded crack remains subsonic and quickly approaches the Rayleigh wave speed. In the mode II case, the crack quickly exceeds the shear wave speed and becomes intersonic. In our particular setting, for which energy is continuously provided to the crack tip region, the crack keeps accelerating and asymptotically approaches the dilatational wave speed $c_d^{(1)}$.

Results for the cross-ply composite(bi-material case) are presented in Fig. 5. Interestingly, results indicate that the maximum delamination speeds under mode-I and mode-II loading are respectively bounded by the shear and dilatational wave speeds of

the more(in-plane) compliant(bottom) material. This result is quite different from that obtained for a Homalite/Aluminum isotropic problem(Breitenfeld and Geubelle, 1998), for which the maximum crack velocity was shown to be the Rayleigh wave speed of the stiffer material. Note that, in that particular case, the Rayleigh wave speed of the stiffer material (Aluminum) exceeded the dilatational wave speed of the more compliant one(Homalite) due to the very strong material mismatch between the two components.

To further illustrate the characteristics of subsonic mode I and intersonic(mode II) crack propagation, Fig. 6 presents the evolution of the main displacement components(normal displacement u_2 in the mode I case, and tangential displacement u_1 in the mode II case) for the 0° unidirectional problems. The various

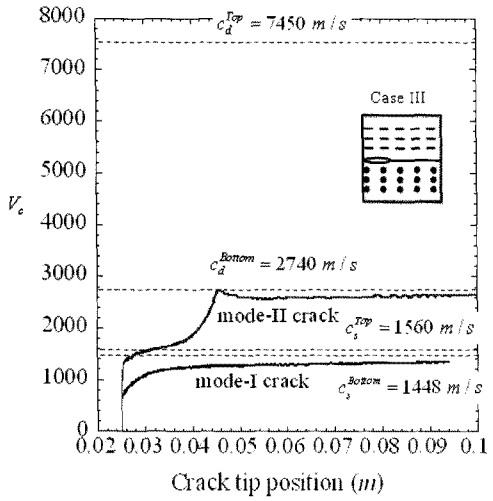

Figure 5 Crack tip speed(V_c) as a function of crack tip position for mode-I and mode-II cracks in bimaterial case.

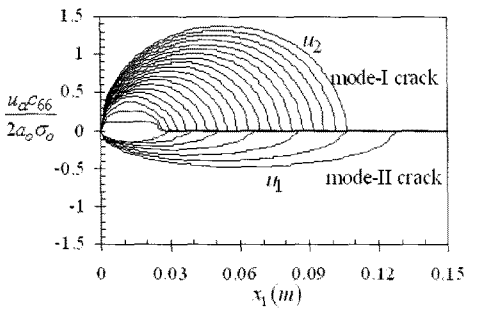

Figure 6 Snapshots of normalized displacement of dynamically propagating mode-I and mode-II cracks in case I: 0° unidirectional graphite/epoxy.

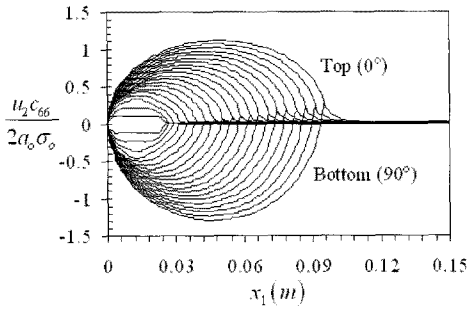

Figure 7 Snapshots of normalized vertical displacement of dynamically propagating mode-I crack in bimaterial case.

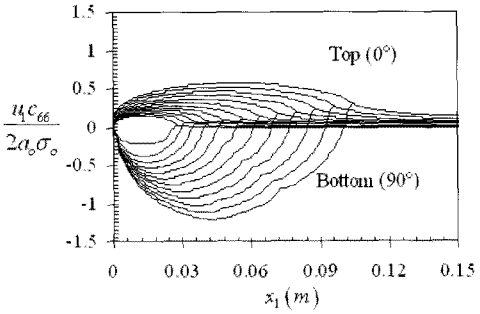

Figure 8 Snapshots of normalized horizontal displacement of dynamically propagating mode-II crack in bimaterial case.

curves are separated by the same time interval of 500 time steps. Taking advantage of mirror(anti) symmetry, both the modes I and II are shown on the same figures. It clearly illustrates the very rapid motion of the mode II crack in the 0° unidirectional case.

Finally, the evolution of the displacements of the top and bottom crack surface obtained during the dynamic delamination process in bimaterial system is presented in Fig. 7(mode I) and 8(mode II). Note the strong asymmetry present in the mode II case between the two components. In the mode I loading case, the top and bottom composite materials offer relatively similar resistance to transverse motion.

4. Conclusions

A spectral scheme has been developed to simulate dynamic fracture in a class of unidirectional and cross-ply fiber-reinforced composites. The method is based on the spectral representation of the transversely isotropic elastodynamic relations between the traction

stresses along the fracture plane and the resulting displacements. It was demonstrated through numerical examples that the spectral method not only captured precisely the subsonic and intersonic crack propagation for mode-I and mode-II cracks. Bimaterial effect on the simulation of dynamic fracture in fiber-reinforced composites was also investigated, showing that the maximum spontaneous debonding speeds under mode I and II in-plane loading conditions are bounded by the lower shear wave and dilatational wave speed of the bimaterial system. This scheme can be directly applicable to the interfacial fracture analysis in the FRP reinforced concrete structures.

References

Abrate, S. (1998) Impact of Composite Structures, Cambridge University Press, NY.

Breitenfeld, M.S., Geubelle, P.H. (1998) Numerical analysis of dynamic debonding under 2D in-plane and 3D loading. *Int. J. Fracture*, 93, pp.13~38.

Broberg, K.B. (1999) Intersonic crack propagation in an orthotropic material, *Int. J. Fracture*, 99, pp.1~11.

Coker, D., Rosakis, A.J. (1998) Experimental observations of intersonic crack growth in asymmetrically loaded unidirectional composites plates, GALCIT SM Report 98-16, Caltech. *Philosophical Magazine A* (2000).

Geubelle, P.H., Baylor, J. (1998) Impact-induced delamination of composites: 2D simulation, *Composites B*, 29B, pp.589~602.

Geubelle, P.H., Breitenfeld, M.S. (1997) Numerical analysis of dynamic debonding under anti-plane shear loading, *Int. J. Fracture*, 85, pp.265~282.

Geubelle, P.H., Kubair, D. (2001) Intersonic crack propagation in homogeneous media: Numerical analysis, *J. Mech. Physics Solids*. 49(3), pp.571~587.

Geubelle, P.H., Rice, J.R. (1995) A spectral method for 3D elastodynamic fracture problems, *J. Mech. Phys. Solids*, 43(11), pp.1791~1824.

Huang, Y., Wang, W., Liu, C., Rosakis, A.J. (1999) Analysis of intersonic crack growth in unidirectional fiber-reinforced composites, *J. Mech. Physics Solids*, 47, pp.1893~1916.

Lambros, J.M., Rosakis, A.J. (1997) An experimental study of the dynamic delamination of thick reinforced polymeric matrix composite laminates, *Experimental Mechanics*, 37(3), pp.360~366.

Rosakis, A.J., Samudrala, O., Coker, D. (1999) Cracks faster than the shear wave speed, *Science*, 284, pp.1337~1340.